

Article

Fabrication of Polypyrrole-Decorated Tungsten Tailing Particles for Reinforcing Flame Retardancy and Ageing Resistance of Intumescent Fire-Resistant Coatings

Feiyue Wang, Hui Liu and Long Yan * 

Institute of Disaster Prevention Science and Safety Technology, School of Civil Engineering, Central South University, Changsha 410075, China; wfyhn@163.com (F.W.); lhui0421@163.com (H.L.)

* Correspondence: ylong015@csu.edu.cn; Tel.: +86-181-6365-0767

Abstract: Polypyrrole-decorated tungsten tailing particles (PPY-TTF) were prepared via the in situ polymerization of pyrrole in the presence of tungsten tailing particles (TTF), and then carefully characterized by Fourier transform infrared spectroscopy (FTIR), scanning electron microscopy (SEM) and thermogravimetric analysis (TG) analyses. The effect of PPY-TTF on the flame retardancy, smoke suppression property and ageing resistance of intumescent fire-resistant coatings was investigated by a fire protection test, smoke density test and cone calorimeter test. The results show that PPY-TTF exerts excellent cooperative effect on enhancing the flame retardancy and smoke suppression properties of the intumescent fire-retardant coatings, which is ascribed to the formation of more cross-linking structures in the condense phase that enhance the compactness and thermal stability of intumescent char. The cooperative effect of PPY-TTF in the coatings depends on its content, and the coating containing 3 wt% PPY-TTF exhibits the best cooperative effect among the samples, showing a 10.7% reduction in mass loss and 35.4% reduction in flame-spread rating compared to that with 3% TTF. The accelerated ageing test shows that the presence of PPY-TTF greatly slows down the blistering and powdering phenomenon of the coatings, thus endowing the coating with the super durability of fire resistance and smoke suppression property. This work provides a new strategy for the resource utilization of tungsten tailing in the field of flame-retardant materials.

Keywords: intumescent fire-retardant coatings; tungsten tailing; fire resistance; anti-ageing performance; cooperative effect



Citation: Wang, F.; Liu, H.; Yan, L. Fabrication of Polypyrrole-Decorated Tungsten Tailing Particles for Reinforcing Flame Retardancy and Ageing Resistance of Intumescent Fire-Resistant Coatings. *Polymers* **2022**, *14*, 1540. <https://doi.org/10.3390/polym14081540>

Academic Editor: Bob Howell

Received: 28 February 2022

Accepted: 5 April 2022

Published: 11 April 2022

Publisher's Note: MDPI stays neutral with regard to jurisdictional claims in published maps and institutional affiliations.



Copyright: © 2022 by the authors. Licensee MDPI, Basel, Switzerland. This article is an open access article distributed under the terms and conditions of the Creative Commons Attribution (CC BY) license (<https://creativecommons.org/licenses/by/4.0/>).

1. Introduction

Intumescent fire-retardant coatings are widely used in high-rise buildings, steel structures, ancient buildings, railway stations, airport terminals and other buildings for the advantages of good finish, small coating thickness, being lightweight, and excellent fire protection performance of the components [1–4], which are considered to be one of the most effective and economical materials to reduce fire hazards on buildings [5,6]. Intumescent fire-retardant coatings generally compose of an intumescent fire-retardant system, binders, synergists, adjuvants and additives, which interact to forge an expanding char layer during combustion that effectively delays the spread of flame and preventing the formation of fire, thus guaranteeing the structural integrity of buildings and minimizing the fire risk [7,8]. Although a large number of studies have concentrated on the enhancement of fire resistance, smoke suppression and reduction in the thickness of intumescent fire-retardant coatings [4,9–11], which neglected the ageing degradation of intumescent fire-retardant coatings under the impacts of environmental factors such as certain humidity, UV radiation, temperature and oxygen.

The use of multifunctional additive is an important strategy to enhance the flame-retardant and smoke suppression efficiencies of intumescent fire-retardant materials. Numerous efforts have investigated the effects of additive on fire resistance, smoke suppression

and ageing resistance of materials, such as SiO₂, bio-fillers, kaolinite, graphene, carbon nanotubes and carbon black [3,6,7,12]. TTF enriches in SiO₂, Al₂O₃, CaO, Fe₂O₃ and other components, which has high chemical stability and small size of particles. However, TTF is easily agglomerated and migrated on the surface of coatings in actual application. To overcome these limitations, many studies have been concentrated on the fabrication of hybrid materials, such as organic space-stabilized polypyrrole latexes and composites with metal oxide or silica particles [13]. Polypyrrole (PPY) has attracted extensive research in supercapacitors, DNA extraction, microwave absorption and contaminant removal, owing to its superior conductivity, easier synthesis, excellent biocompatibility, high thermal stability and non-toxicity [14–18]. The preparation and characterization of silica–polypyrrole nanocomposite colloids using silica particles have been reported by Armes et al. [19]. Among them, silica/PPY nanocomposites have a low cost, high surface area and easier dispersion, which can improve the wear resistance, UV resistance, barrier property, mechanical performance and thermal stability of organic coatings [20]. Copolymerization can be an opportunity to amend the physical properties and avoid the drawbacks of individual polymers, and several copolymer composites may demonstrate better behavior in many applications [21]. Microencapsulation is an important method of enhancing the compatibility of fillers, and the resulting polypyrrole-decorated tungsten tailing particles (PPY-TTF) are expected to have better dispersion in intumescent fire-retardant coatings via the in situ polymerization of pyrrole, thus obtaining better fire resistance and anti-ageing properties.

Herein, a preparation method for PPY-TTF was proposed via the in situ polymerization of pyrrole in the presence of TTF particles. Five intumescent fire-retardant coatings were prepared with an intumescent fire-retardant system, waterborne epoxy resin and PPY-TTF. The effect of PPY-TTF on the combustion performance of intumescent fire-retardant coatings was analyzed by various analytical methods, and the flame-retardant and smoke suppression mechanisms of PPY-TTF were also proposed.

2. Experimental Section

2.1. Materials

TTF was obtained from Hunan Anhua Xiangnan Tungsten Co., Ltd., Hunan, China. Waterborne epoxy hardener (ERC 2610, amine value: 180 ± 40 mg KOH/g) and waterborne epoxy resin (ERE 2581, solid content: $52 \pm 1\%$) were supplied from Ruicheng Selected New Materials Technology Co., Ltd., Guangdong, China. Pyrrole (C₄H₅N, purity: 99%) and FeCl₃·6H₂O (purity: 99.0%) were offered by Shanghai Aladdin Biochemical Technology Co., Ltd., Shanghai, China. The pentaerythritol (PER, purity: 99.5%), ammonium polyphosphate (APP, water solubility $\leq 0.04\%$, purity: 99.5%) and melamine (MEL, purity $\geq 99.5\%$) were available from Hangzhou JLS Flame Retardant Chemical Co., Ltd., Hangzhou, China. The acrylate copolymer carboxylate used as a dispersant was supplied by Qingdao Xingguo Coatings Co., Ltd., Qingdao, China. The non-silicon defoamer was supplied by Qingdao Xingguo Coatings Co., Ltd., Qingdao, China.

2.2. Preparation of Polypyrrole-Decorated Tungsten Tailing Filler

Firstly, 30 g TTF was added to 400 mL mixture of anhydrous ethanol and water (2:8) and ultrasonicated for 0.5 h. One milliliter pyrrole was dropped into the solution and dispersed ultrasonically for 10 min. Owing to the charge interaction between the pyrrole and TTF, the pyrrole monomers in solution migrated to the surface of TTF particles. Then, 7.99 g FeCl₃·6H₂O was mixed with 100 mL water, stirred to dissolve and sonicated to disperse. The FeCl₃·6H₂O solution was slowly dropped into the above solution and the reaction occurred at low temperature, with stirring for 24 h to polymerize the pyrrole monomers on the surface of TTF particles. The PPY-TTF was obtained by extracting and drying at 60 °C for 6 h. The synthetic route of PPY-TTF is shown in Figure 1.

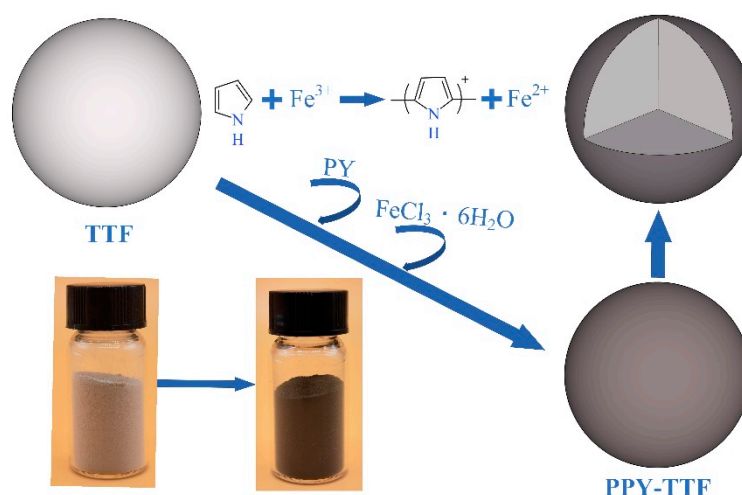


Figure 1. Synthetic route of PPY-TTF.

2.3. Preparation of the Intumescent Fire-Retardant Coatings

The intumescent flame retardant (IFR) was obtained by mixing APP, PER and MEL with a mass ratio of 3:1.5:1, which was combined with PPY-TTF and deionized water according to the formula in Table 1 and then stirred at 1000 r/min for 20 min. Then, waterborne epoxy resin, defoamer and dispersant were put into the slurry stirring at 500 r/min for 20 min. Finally, the waterborne epoxy hardener was added and stirred at 500 r/min for 20 min to obtain the intumescent fire-retardant coatings. The intumescent fire-retardant coatings with different amounts of PPY-TTF are named IFRC₀-IFRC₅, and the specific test formulations are shown in Table 1.

Table 1. Compositions of the intumescent fire-retardant coatings %.

Samples	IFR	TTF	PPY-TTF	Waterborne Epoxy Resin	Defoamer	Dispersant	Waterborne Epoxy Hardener
IFRC ₀	55	0	0	40	0.5	0.5	4
IFRC ₁	54	0	1	40	0.5	0.5	4
IFRC ₂	53	0	2	40	0.5	0.5	4
IFRC ₃	52	0	3	40	0.5	0.5	4
IFRC ₄	50	0	5	40	0.5	0.5	4
IFRC ₅	52	3	0	40	0.5	0.5	4

2.4. Characterization

2.4.1. Fourier Transform Infrared Spectroscopy

Fourier transform infrared spectroscopy (FTIR) spectra were characterized by an iCAN9 FTIR spectrometer using KBr pellets (Tianjin Energy Spectrum Technology Co., Ltd., Tianjing, China).

2.4.2. Scanning Electron Microscopy

The MIRA 3 LMU scanning electron microscopy (Tescan, Brno, Czech Republic) was used to characterize the micromorphology of the samples at a voltage of 20.0 kV.

2.4.3. X-ray Diffraction

X-ray diffraction (XRD) pattern was characterized by an Advance D8 XRD diffractometer at a range of 3 to 70°, a Cu-K α radiation and a rate of 5°/min (Bruker, Fällanden, Switzerland).

2.4.4. X-ray Fluorescence Spectrometer

X-ray fluorescence spectrometer (XRF) analysis was performed with a ZSX Primus II X-ray Fluorescence Spectrometer (Rigaku, Japan).

2.4.5. Smoke Density Test

Smoke density test was performed on a PX-07-008 smoke density tester for building materials (Phoenix Quality Inspection Instruments Co., Ltd., Suzhou, China).

2.4.6. Fire Protection Tests

Fire protection properties of the samples were assessed by the big panel method, cabinet method, tunnel method tests according to GB12441-2018 standard procedure. The big panel method test was conducted on a MT-X multiplex temperature recorder (Shenzhen Shenhwa Technology Co., Ltd., Shenzhen, China) to obtain the backside-temperature curves of coating samples.

Cabinet method test was carried out on an XSF-1 apparatus, the weight loss (the difference in the sample mass before and after the test), char index and intumescent factor (the ratio of the thickness of the coatings after and before test) of the samples were determined. The char index was calculated by Formula (1):

$$\text{Char index} = \frac{\sum_{i=1}^n (a_i b_i h_i)}{n} \quad (1)$$

where a_i is defined as the char length (cm), b_i is defined as the char width (cm), h_i is defined as the char depth (cm) and n is the number of samples.

Tunnel method test was conducted on a SDF-2-type 2-foot flame tunnel instrument (Jiangning Analysis Instrument Company, Nanjing, China). The flame spread over the coating surface of the samples was evaluated when ignited under controlled conditions in a small tunnel, and the flame-spread rating of the samples was calculated by Formula (2):

$$\text{FRS} = \frac{L_s - L_a}{L_r - L_a} \quad (2)$$

where L_s is the mean of five flame advance readings of samples (mm), L_a is the mean of five flame advance readings of asbestos board (mm) and L_r is the mean of five flame advance readings of oak board (mm).

2.4.7. Adhesion Classification Test

The adhesion classification test was carried out on a QFH-HD600 adhesion tester to test the coating adhesion (Changzhou Edex Instruments Co., Ltd., Changzhou, China) on the basis of ASTM D 3359-09.

2.4.8. Pencil Hardness Test

The pencil hardness test was performed on a QHQ-A portable pencil scratch tester in accordance with ISO 15184-2012. The lead of a pencil was vertically erected and polished on sandpaper for a flat and round cross-sectioned end. The pencil hardness of the coating was tested progressively by placing a polished pencil on the coating at an angle of 45° under a load of 750 g.

2.4.9. Cone Calorimeter Test

The cone calorimeter test was used to characterize the heat release rate (HRR) and total heat release (THR) curves of coatings with an external heat flux of 50 kW/m².

2.4.10. Thermogravimetric Analysis

TG analysis was carried out on a TGA/SOTA 851 thermogravimetric instrument (Mettreoli Instruments Co., Ltd., Zurich, Switzerland) from 30 °C to 800 °C at a heating

rate of 10 °C/min under a nitrogen atmosphere. The theoretical char residue (W_{theo}) of IFRC₀-IFRC₅ samples was calculated using Formula (3):

$$W_{\text{theo}}(t) = \sum_{i=1}^n \chi_i W_i(t) \quad (3)$$

where $W_i(t)$ is the amount of residual char for i at t °C; χ_i is the percentage of i , %.

2.4.11. Accelerated Ageing Test

The accelerated ageing test was performed on an UV-accelerated ageing tester (Shi Haoran Machinery Equipment Factory, Dongguan, China) according to ASTM G154-2006. One ageing cycle included 12 h, during which, the condensation time was 4 h at 50 ± 3 °C, and the UV exposure was 8 h at 60 ± 3 °C with an irradiation of 0.76 W/(m²·nm). The samples were exposed to accelerated ageing tests for 2, 6 and 11 cycles, accompanying with the change of sample position every 12 h.

3. Results and Discussion

3.1. Morphology and Composition of TTF and PPY-TTF

The XRD patterns of TTF are presented in Figure 2. From Figure 2, the XRD patterns of TTF samples are generally consistent with the standard patterns of quartz (SiO₂) (PDF85-0794). The major diffraction peaks located at 21.0°, 26.8°, 36.7°, 39.6°, 40.5°, 42.7°, 46.0°, 50.3°, 55.1°, 55.5°, 60.1°, 64.2°, 67.9° and 68.3° are attributed to (100), (011), (110), (102), (111), (200), (201), (112), (022), (013), (121), (113), (122) and (203) phases of SiO₂, indicating that the main component of TTF is SiO₂. XRF is used for analyzing the elemental composition of TTF, and the results are illustrated in Table 2. From Table 2, it is clearly seen that the main component of TTF is SiO₂, which is in agreement with the XRD result.

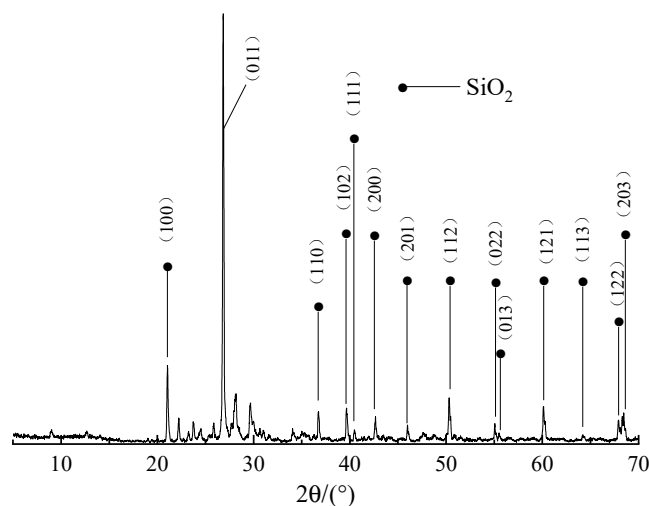


Figure 2. XRD patterns of TTF.

Table 2. XRF test of TTF.

Components	SiO ₂	Al ₂ O ₃	CaO	MnO	Fe ₂ O ₃	MgO	Na ₂ O	K ₂ O	WO ₃	SO ₃
Content/%	60.2	10.4	11.8	2.4	6.7	1.6	0.8	1.8	0.4	2.8

Figure 3 exhibits the SEM images and EDS maps of TTF and PPY-TTF. From Figure 3a, it can be seen that the TTF sample shows irregular blocky structures with a size range of 10 and 50 μm. Compared to TTF, the size of PPY-TTF is obviously reduced, showing a smaller agglomeration phenomenon. From EDS maps, C and N elements from polypyr-

role are homogeneously distributed on the surface of TTF, indicating that PPY-TTF was prepared successfully.

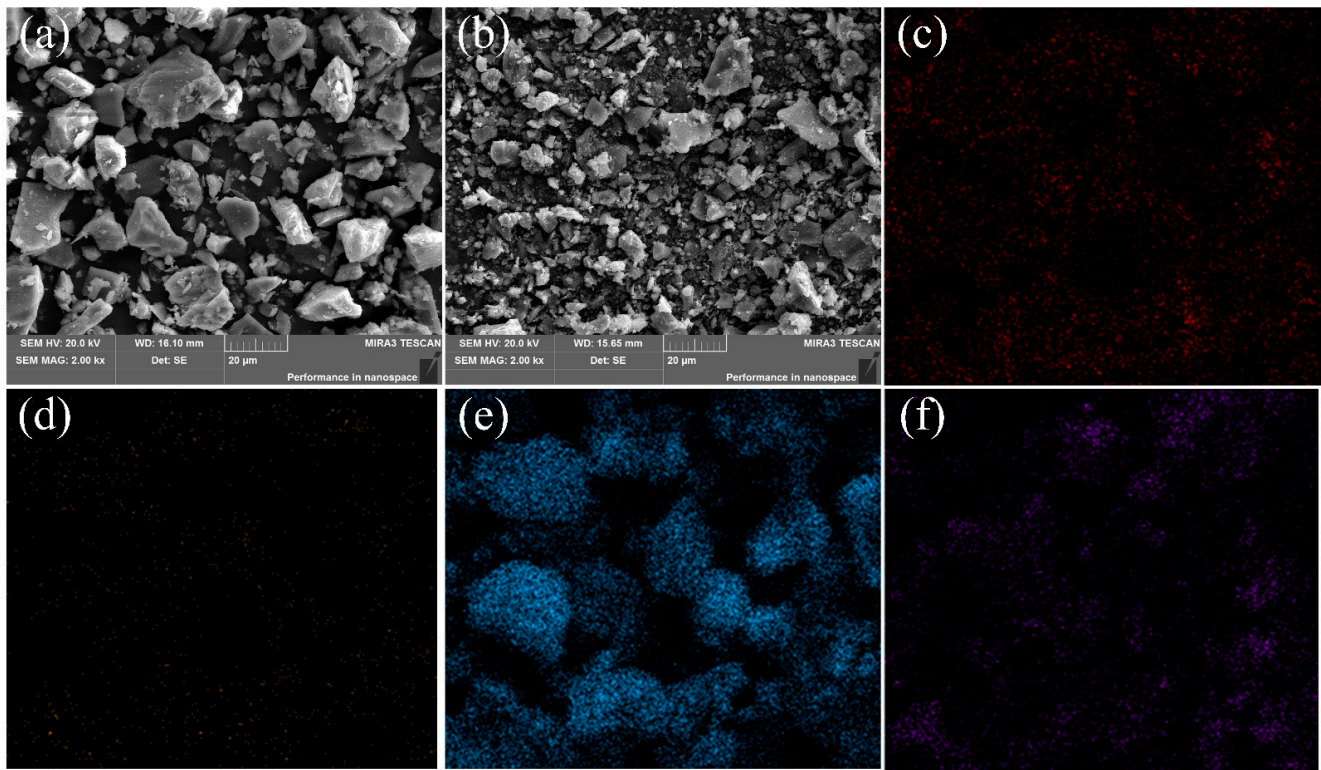


Figure 3. SEM and EDS; (a) SEM of TTF; (b) SEM of PPY-TTF; (c) carbon; (d) nitrogen; (e) silicon; (f) ferrum.

Figure 4 shows the FTIR spectra of TTF and PPY-TTF. In the spectrum of TTF, the characteristic peaks at 1005, 777 and 459 cm^{-1} are attributed to the symmetric and anti-symmetric stretching vibration peaks of Si-O-Si [22,23]. As for PPY-TTF, the new peaks of the C-H stretching vibration ($2928, 2859\text{ cm}^{-1}$), C=C stretching vibration (1631 cm^{-1}) and C-N and N-H stretching vibration (1551 cm^{-1}) are observed [23–25], further confirming polypyrrole was successfully decorated on the surface of TTF particles.

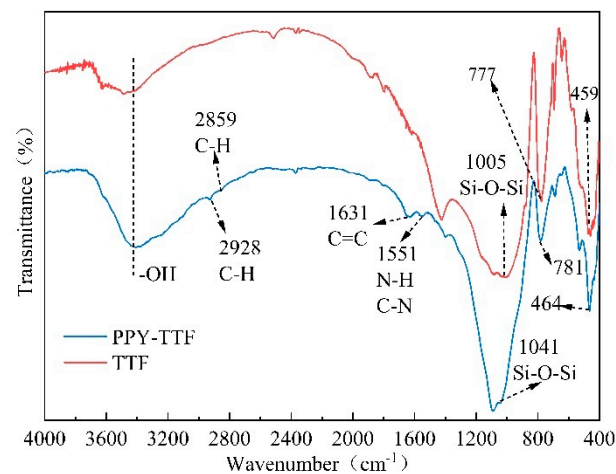


Figure 4. FTIR spectra of TTF and PPY-TTF.

Figure 5 shows the TG and differential thermo-gravimetric (DTG) curves of TTF and PPY-TTF. From the TG and DTG curves of TTF, it can be seen that the pyrolysis

process of TTF is mainly from 420 °C to 800 °C concomitant with a strong DTG peak and a residual weight of 96.0% at 800 °C. Meanwhile, the pyrolysis process of PPY-TTF is mainly divided into four stages. The first stage corresponds to the temperature interval of 26–200 °C, which is due to physics-absorbing water molecules, oligomer molecules and volatile impurities. The second stage at 200–430 °C is attributed to the degradation of low molecular-weight polymer chains. The third stage at 430–560 °C is the decomposition stage of polypyrrole. The fourth stage at 560–800 °C is the decomposition stage of TTF and polypyrrole, remaining an 81.8% residue at 800 °C.

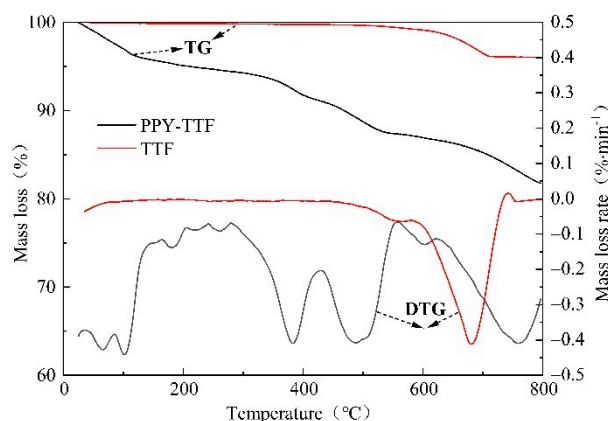


Figure 5. TG and DTG curves of TTF and PPY-TTF.

3.2. Fire Protection Tests

The results of the tunnel method and cabinet method tests are given in Table 3. The mass loss, charring index, flame-spread rating and intumescent factor of IFRC₀ samples are 3.7 g, 34.9 cm³, 20.5 and 25.0, respectively, while the addition of PPY-TTF can significantly enhance the fire resistance of the intumescent fire-retardant coatings. In particular, IFRC₃ presents the best heat-insulation performance, with a 32.9% reduction in weight loss, 46.7% reduction in charring index, 74.3% reduction in flame-spread rating and 80.0% increase in intumescent factor compared with IFRC₀. The results indicate that the appropriate amount of PPY-TTF obtained via the in situ polymerization of pyrrole can effectively strengthens the fire protection of coatings. In addition, an excessive amount of PPY-TTF may suppress the expansion and carbonization of the coatings, thus diminishing its cooperative fire resistance in intumescent fire-retardant coatings.

Table 3. Fire protection performance of intumescent fire-retardant coatings.

Samples	IFRC ₀	IFRC ₁	IFRC ₂	IFRC ₃	IFRC ₄	IFRC ₅
Mass loss/g	3.7 ± 0.1	3.4 ± 0.1	3.0 ± 0.1	2.5 ± 0.1	2.8 ± 0.1	2.8 ± 0.1
Charring index/cm ³	34.9 ± 0.6	29.9 ± 0.8	23.8 ± 2.4	18.6 ± 0.8	19.6 ± 0.4	18.1 ± 0.4
Flame-spread rating	20.5 ± 1.7	15.8 ± 2.9	8.2 ± 0.8	5.3 ± 2.9	8.2 ± 0.8	8.2 ± 0.3
Intumescent factor	25.0 ± 4.1	31.7 ± 2.4	37.5 ± 2.4	45.0 ± 4.1	42.5 ± 4.1	41.7 ± 2.4

Figure 6 shows the backside temperature curves of the substrates coated with IFRC₀–IFRC₄ coatings. As demonstrated in Figure 6, the backside temperature of the IFRC₀ sample without PPY-TTF rises rapidly, with a fire resistance time of 800 s, corresponding to a poor heat-insulation performance. The backside temperature of IFRC₁–IFRC₄ samples containing PPY-TTF has a slower rise and becomes stable at about 500 s. The equilibrium backside temperatures of the samples at 900 s are 180.0, 167.7, 142.3 and 156.2 °C, respectively, indicating that the presence of PPY-TTF enhances the fire protection of the coatings. Among them, the IFRC₃ sample presents the best fire-retardant effect, which is consistent with the results in Table 3.

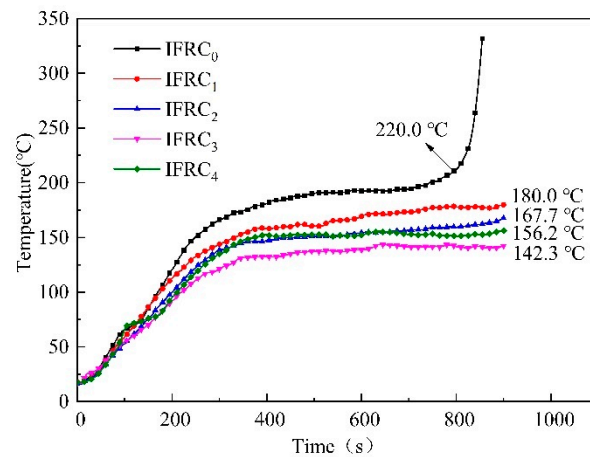


Figure 6. The backside-temperature curves of the substrates coated with IFRC₀–IFRC₄ coatings.

Figure 7 exhibits digital photographs of the char layers after the smoke density test, where the IFRC₀ char presents the smallest expansion height and the poorest surface structure, thus showing the worst fire-retardant properties. After the addition of PPY-TTF, the char layer heights of IFRC₁–IFRC₄ are 8.5 mm, 11.5 mm, 14.5 mm and 12.5 mm, respectively, revealing that the presence of PPY-TTF enhances the carbonization and expansion process of the coatings. In particular, the IFRC₃ sample exhibits the highest intumescent factor and the densest char. From the SEM images of Figure 8, it can be found that the introduction of PPY-TTF facilitates the formation of a denser and more continuous char layer structure without obvious holes or other defects that effectively blocks the transfer of combustible materials and heat. From the EDS maps of Figure 8, the higher content of P and Si elements in IFRC₃ are observed, which indicate that the presence of PPY-TTF is favorable to the formation of more phosphorus-rich and silicon-rich cross-linking structures that enhance the heat-insulation performance of the char layer. Moreover, the char layer of IFRC₃ has a higher C/O mass ratio compared to that of IFRC₀, resulting in a good oxidation resistance and fire resistance [7].

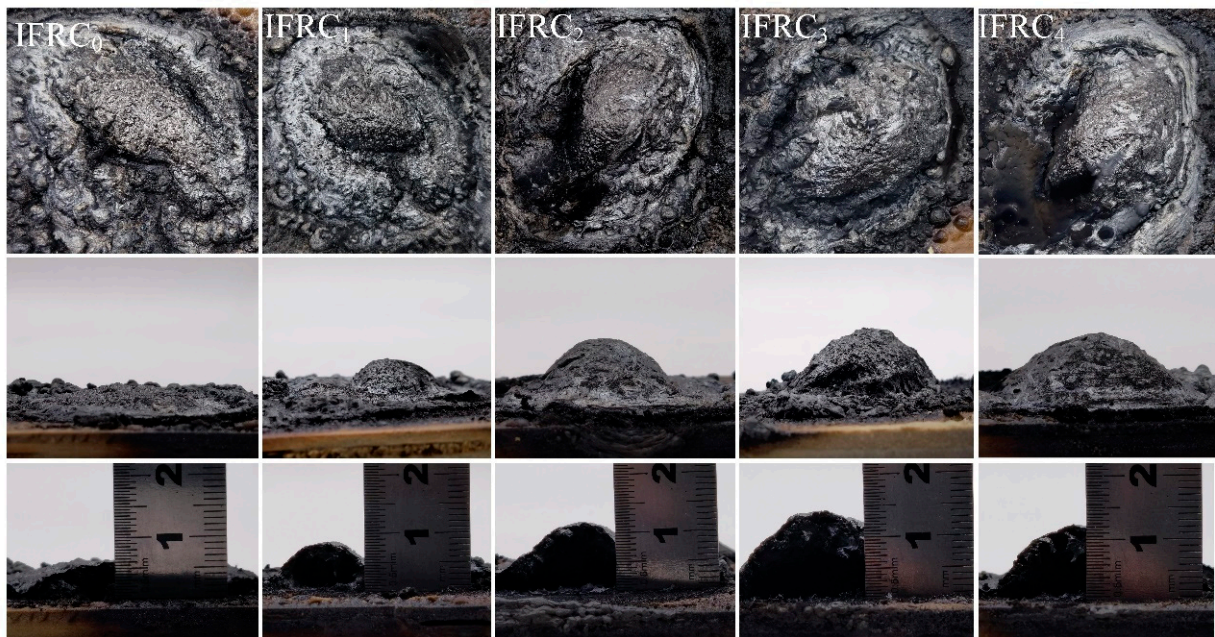


Figure 7. Digital photographs of the obtained char layers from IFRC₀–IFRC₄.

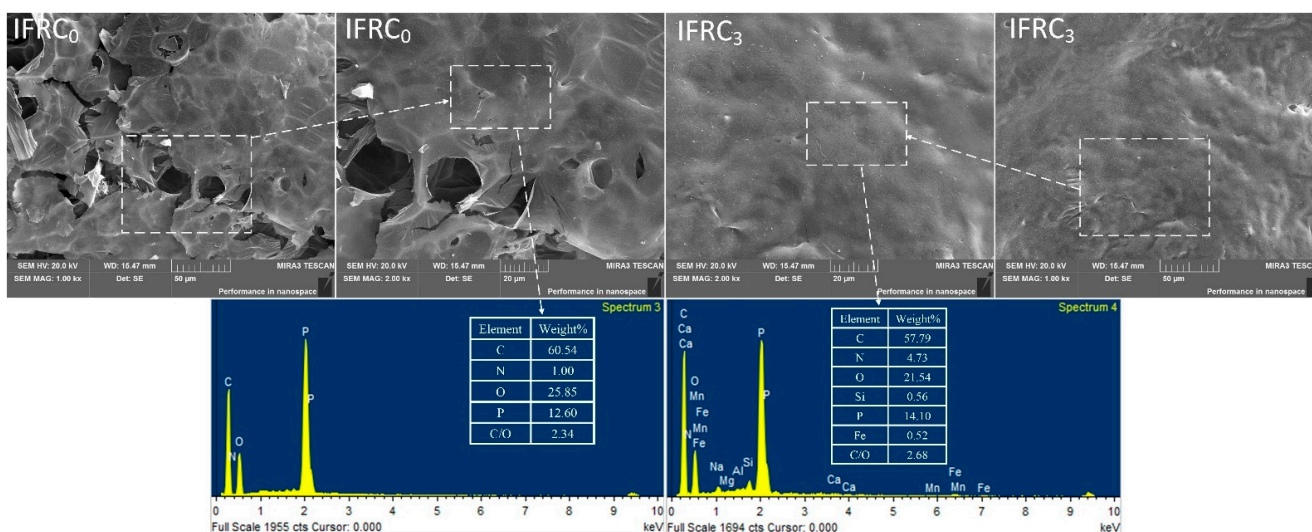


Figure 8. SEM-EDS maps of IFRC₀ and IFRC₃.

3.3. Cone Calorimeter Test

The THR and HRR curves of the IFRC₀–IFRC₄ samples are presented in Figures 9 and 10, respectively. As depicted in the figures, the samples illustrate two peaks due to the decomposition of the char layer and the plywood. The first peak heat release rate (PHRR1) of IFRC₀ is 108.5 kW/m² appeared at 21 s. With the addition of PPY-TTF, both THR and PHRR values of IFRC₁–IFRC₄ coatings are significantly reduced. Compared with IFRC₀, the THR and PHRR1 values are reduced by 5.9% and 12.1% for IFRC₁, 13.5% and 18.5% for IFRC₂, 21.6% and 31.2% for IFRC₃ and 10.9% and 27.2% for IFRC₄, suggesting that the presence of PPY-TTF can effectively improve flame retardancy of the coating. Moreover, the coatings containing PPY-TTF show lower second peak heat release rate (PHRR2) compared to the coating without PPY-TTF, indicating better flame inhibition effect on wood substrates. In conclusion, the coatings containing PPY-TTF can significantly reduce the THR and HRR of coating samples, among which, the IFRC₃ has the best performance. This phenomenon is mainly attributed to the fact that PPY-TTF can effectively promote the char formation of the coating and strengthen the structure of the char layer, thus effectively delaying the transfer of heat and mass between the flame and the substrates. However, the cooperative effect of PPY-TTF in the coatings depends on the amount of PPY-TTF. When the amount of PPY-TTF exceeds 3 wt%, the cooperative fire-retardant effect will be weakened, which is ascribed to an excessive content of PPY-TTF may solidify the molten char layer that inhibits the char formation process [20].

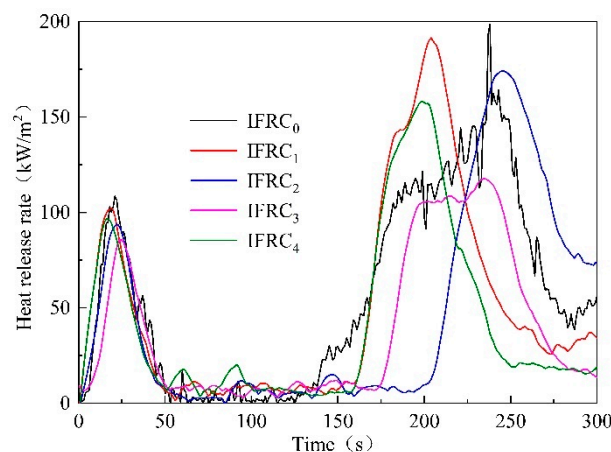


Figure 9. HRR curves of IFRC₀–IFRC₄ samples.

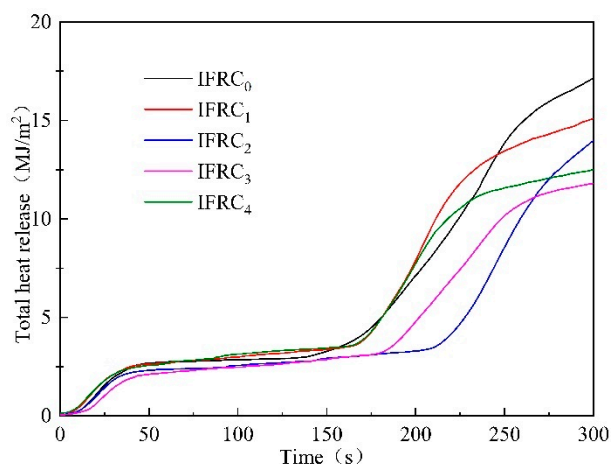


Figure 10. THR curves of IFRC₀–IFRC₄ samples.

3.4. Smoke Density Test

Figure 11 presents the light absorption curves and smoke density rating (SDR) values of the wood substrates coated with intumescent fire-resistant coatings. The maximum light absorption values of IFRC₀–IFRC₄ are 59.0%, 56.2%, 52.2%, 40.6% and 47.7%, and the smoke density rating values are 33.3%, 31.3%, 24.4%, 22.5% and 23.6%, respectively. The addition of PPY-TTF can effectively reduce the smoke density rating values and light absorption rate of coatings, among which the IFRC₃ sample shows the optimal smoke suppression performance. The super smoke suppression effect of PPY-TTF in the coating is ascribed to the formation of a dense and compact char against the release of pyrolysis products during combustion.

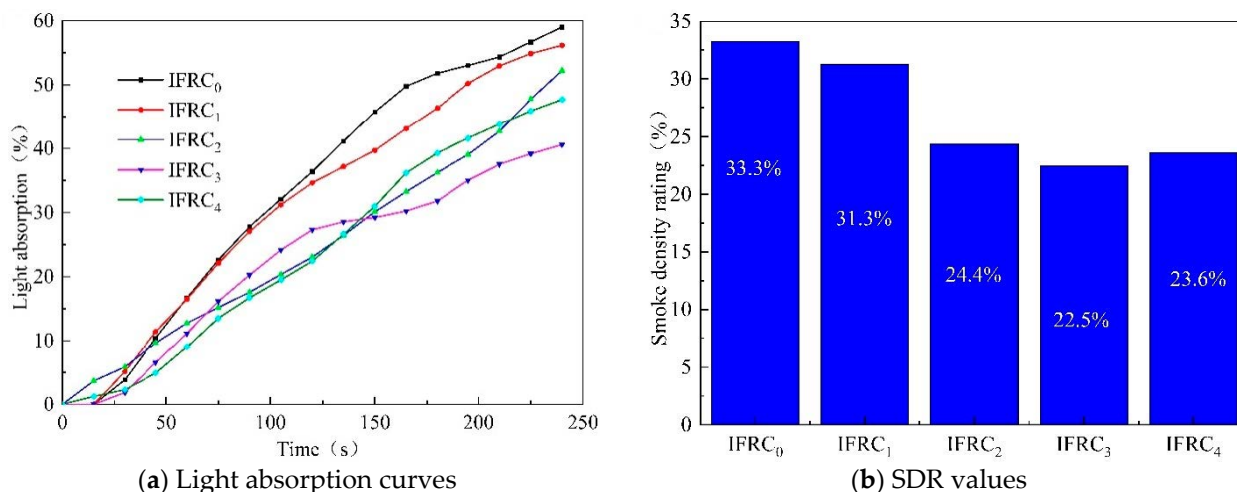


Figure 11. Light absorption curves and SDR values of IFRC₀–IFRC₄ samples.

3.5. Thermal Stability Analysis

The TG and DTG curves of coatings under a nitrogen atmosphere are depicted in Figure 12. As seen in Figure 12, the decomposition process of the coating is mainly divided into four stages in the temperature range of 100–300 °C, 300–430 °C, 430–580 °C and 580–800 °C, respectively. The first stage is mainly the stage of dehydration, volatilization for small molecules and low temperature decomposition of IFR with lower mass loss. As the temperature continues to rise, the second stage appears a strong DTG peak accompanied with a higher mass loss, which is mainly caused by the decomposition of the cured epoxy resin and APP, PER and MEL. In this stage, APP decomposes to generate polyphosphoric acid and phosphoric acid derivatives that promote the esterification of PER into char, while polyphosphoric acid dehydrates to form a cross-linking structure. The NH₃ and H₂O

released from MEL and APP in this process can promote the expansion of the char layer. In the third stage, the formed cross-linking structures and polypyrrole are degraded at a large scale. The fourth stage is ascribed to the decomposition of unstable char layer at a high temperature, accompanying with a mass loss of about 1.5%.

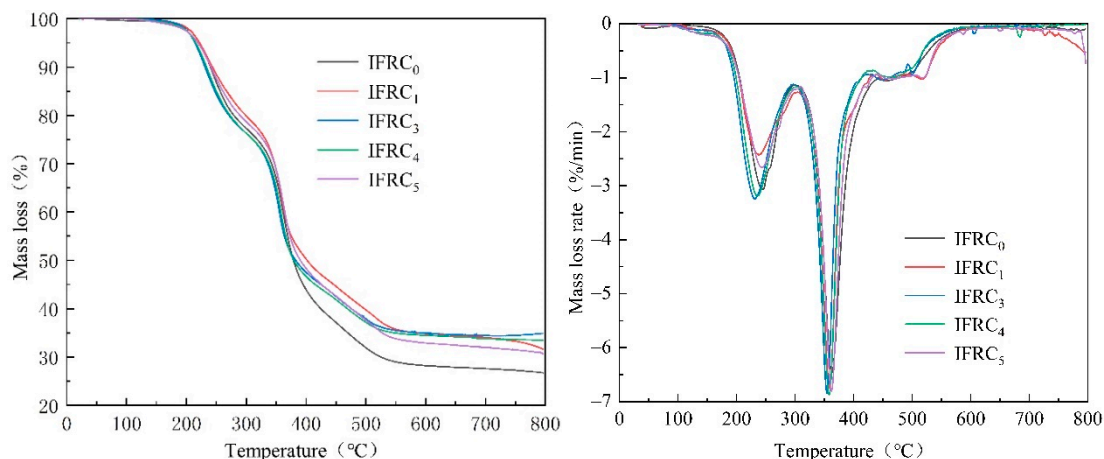


Figure 12. TG and DTG curves of intumescent fire-retardant coatings.

Table 4 illustrates the relevant thermal decomposition parameters. As seen in Table 4, T_0 and T_m values of IFRC₀ sample occur at 223.1 °C and 362.9 °C, respectively, and the residual weight at 800 °C is 26.7%. With the addition of PPY-TTF, the coatings show lower T_0 , T_m and mass loss, suggesting a reduction in the release of pyrolysis products and an increase in the amount of residual char. Generally, the higher the ΔW value of the sample, the stronger the interaction between the components. After adding PPY-TTF, the W_{exp} of the specimens is significantly higher than their W_{theo} . Among them, IFRC₃ shows the maximum ΔW value of 15.9% corresponding to the best char-forming efficiency. The results indicate that PPY-TTF can effectively improve the structure of the char layer and encourage the cross-linking reaction of degradation products to strengthen the thermal stability and char-forming ability of coatings, thus exhibiting a super cooperative effect.

Table 4. The relevant thermal decomposition parameters of intumescent fire-retardant coatings.

Samples	T_0 / °C	T_m / °C	PMLR/ (%/min)	W_{exp} (800 °C)/%	W_{theo} (800 °C)/%	ΔW (800 °C)/%
IFRC ₀	223.1	362.9	6.5	26.7	16.8	9.5
IFRC ₁	222.2	359.1	6.7	31.6	17.4	14.2
IFRC ₃	214.3	354.7	6.8	34.9	19.0	15.9
IFRC ₄	215.8	358.1	6.9	33.5	20.6	12.9
IFRC ₅	219.3	362.0	6.8	30.6	19.4	11.2

Notes: T_0 , the temperature of initial decomposition with the mass loss of 5%; PMLR, peak mass loss rate; T_m , the temperature of PMLR; W_{exp} , the experimental char residue; $\Delta W = W_{exp} - W_{theo}$; W_{exp} of the cured epoxy resin, IFR, TTF, PPY-TTF at 800 °C were 6.7%, 25.2%, 96.0%, 81.8%, respectively.

3.6. Accelerated Ageing Test

Figure 13 presents the morphologies of the IFRC₀ and IFRC₃ samples before and after the ageing treatment. With the increased ageing time, the obvious blistering, powdering and yellowing phenomena appear on the surface of the IFRC₀ coating. The powdering phenomenon is caused by the precipitation and decomposition of IFR under the influence of UV irradiation and hydrothermal conditions, whereas the blistering phenomenon mainly results from the reduction of the adhesion of the coatings. Figure 14 exhibits the adhesion classification and pencil hardness of IFRC₀ and IFRC₃ coatings after the accelerated ageing treatment. As shown in Figure 14, the adhesion classification and pencil hardness of the

coatings gradually weakened with the increase of ageing cycles. However, the IFRC₃ coating has a better performance than that of IFRC₀ under the same ageing treatment. This may be explained by the reason that the introduction of PPY-TTF can effectively strengthen the hardness, adhesion and shielding effect of the coating and weaken the ageing degradation of the coatings, thus exhibiting less bubbles and the precipitation of flame retardants, as seen in Figure 13. Therefore, the addition of PPY-TTF can effectively enhance the durability of the coating and slow down the blistering, powdering and yellowing of the coatings.

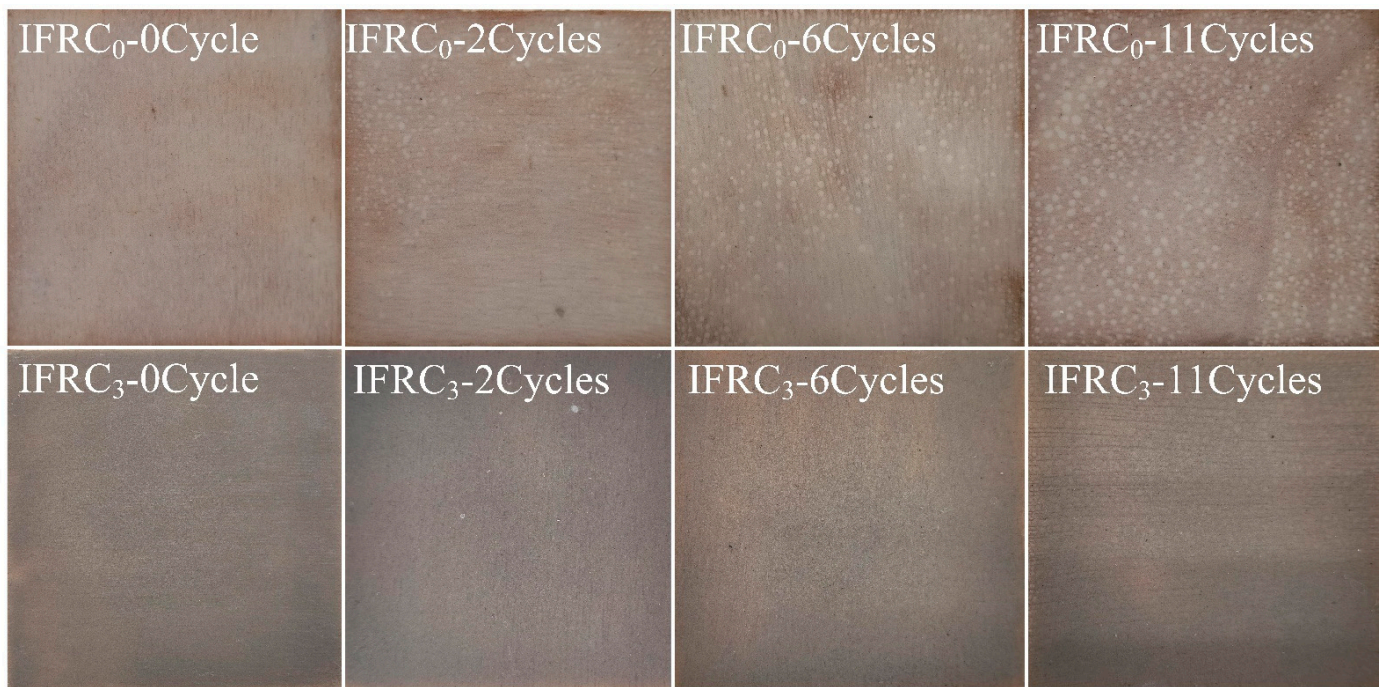


Figure 13. Digital photos of IFRC₀ and IFRC₃ after different ageing cycles.

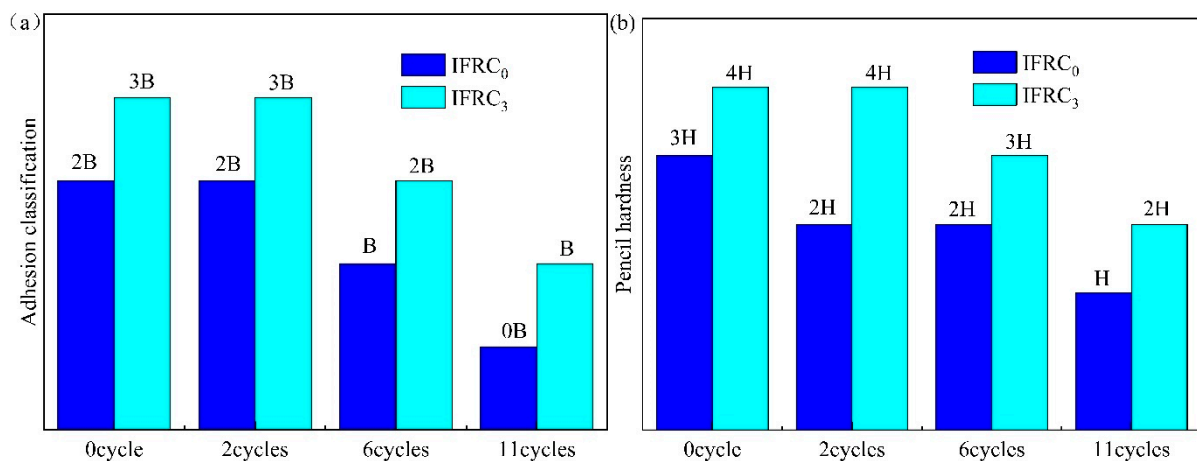


Figure 14. Adhesion classification (a) and pencil hardness (b) of IFRC₀ and IFRC₃ after different ageing cycles.

The smoke emission characteristics of IFRC₀ and IFRC₃ coatings before and after ageing treatment are presented in Figure 15. As depicted in Figure 15, the maximum light absorption rating and SDR values of IFRC₀ and IFRC₃ samples gradually increase with the growth of the ageing cycle, reflecting the increase of smoke production. Compared with IFRC₀, the IFRC₃ sample still expresses a better cooperative smoke-suppression effect after the same accelerated ageing treatment, which is ascribed to the enhanced integrity of

the coatings after introduction of PPY-TTF under ageing treatment. It can be concluded that the presence of PPY-TTF can strengthen the durability of smoke-suppression effect of intumescent fire-retardant coatings.

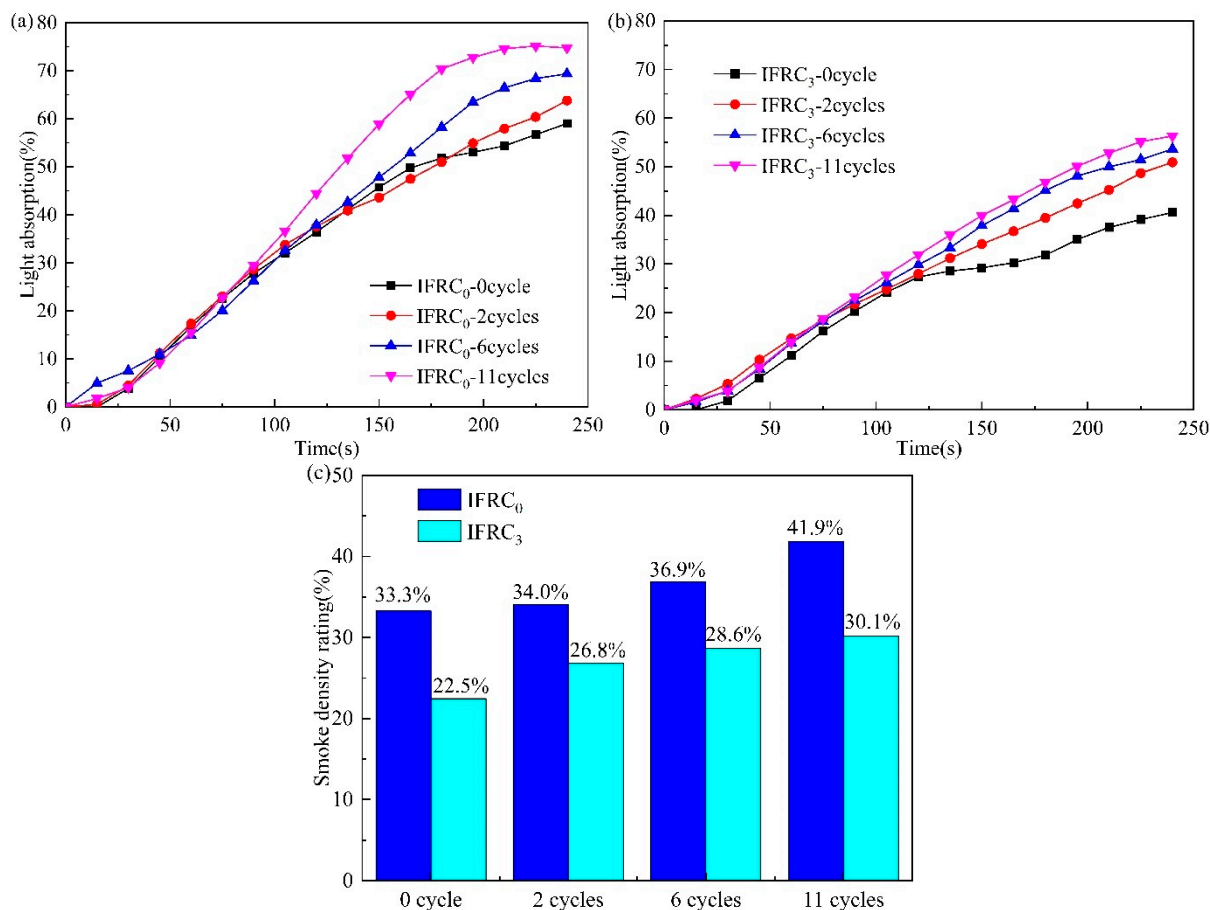


Figure 15. Smoke density testing results after different ageing cycles; (a) light absorption of IFRC₀; (b) light absorption of IFRC₃; (c) SDR of IFRC₀ and IFRC₃.

The fire resistance of IFRC₀ and IFRC₃ samples after the ageing treatment are given in Figure 16. As shown in Figure 16, IFRC₀ and IFRC₃ have a reduction in fire-retardant time with the increase of ageing time, indicating that the degradation of fire protection performance. Compared with IFRC₀, the ageing process has a less negative effect on the fire resistance of IFRC₃ coating. The reason is that the addition of PPY-TTF is beneficial to weaken the migration of flame retardants and morphology deterioration of the coatings, thus imparting the coatings with a long-term durability of fire resistance.

Intumescent fire-retardant coatings are susceptible to photo-oxidation and thermal oxidation in daily use, and the evolution processes of coatings under ageing conditions are monitored by FTIR analysis. Figure 17 presents the FTIR spectra of IFRC₀ and IFRC₃ coatings, and Table 5 gives the functional groups of IFRC₀ and IFRC₃ samples after different ageing cycles. As observed in Figure 17 and Table 5, the absorption peaks of $-\text{NH}_2$ ($3470, 3419, 1439 \text{ cm}^{-1}$), $\text{C}=\text{N}$ (1654 cm^{-1}), $\text{N}-\text{H}$ ($1552, 3134 \text{ cm}^{-1}$), $\text{P}=\text{O}$ (1249 cm^{-1}) and $\text{C}-\text{O}$ (1016 cm^{-1}) groups are obviously strengthened with the increase in the ageing cycle [24,26–32], indicating that flame retardant migrates to the surface of the coating under the influence of ageing factors such as irradiation, oxygen, humidity and temperature. However, after eleven ageing cycles, the intensity of the absorption peaks for $-\text{NH}_2$, $\text{C}=\text{N}$, $\text{N}-\text{H}$, $\text{P}=\text{O}$, and $\text{C}-\text{O}$ functional groups decrease remarkably and the $-\text{NH}_2$ and $\text{N}-\text{H}$ groups disappear, showing that the migration, hydrolyzation and oxidation of APP, PER and MEL under ageing conditions. Compared with IFRC₀, the IFRC₃ coating has stronger

absorption vibration peaks for the main functional groups under the same ageing treatment, corresponding to a weaker ageing degradation. This result shows that PPY-TTF can strengthen the structural stability of the coatings and reduce the migration, hydrolization and oxidation of the coatings during ageing conditions, thus endowing the coatings with a better ageing resistance.

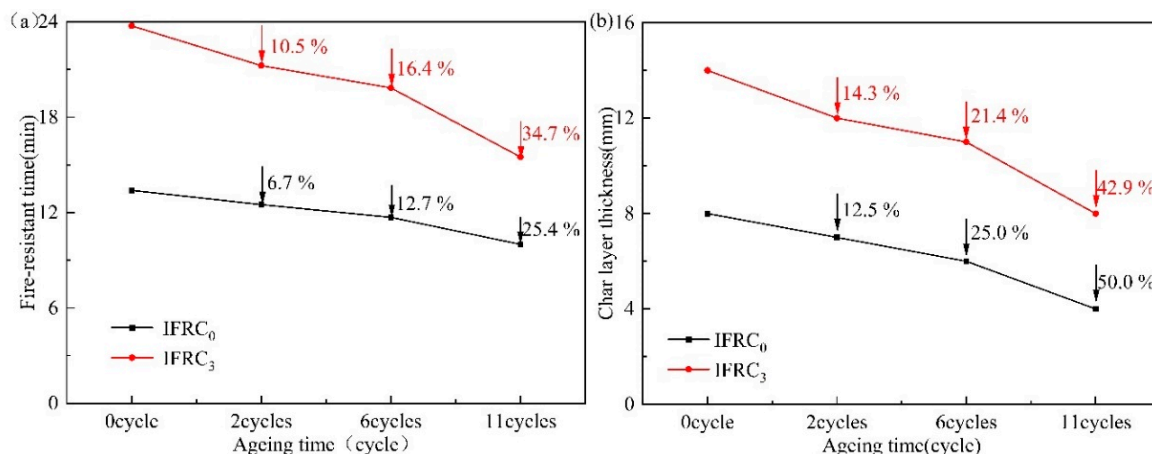


Figure 16. Fire-resistant time (a) and char layer thickness (b) of IFRC₀ and IFRC₃ after accelerated ageing test.

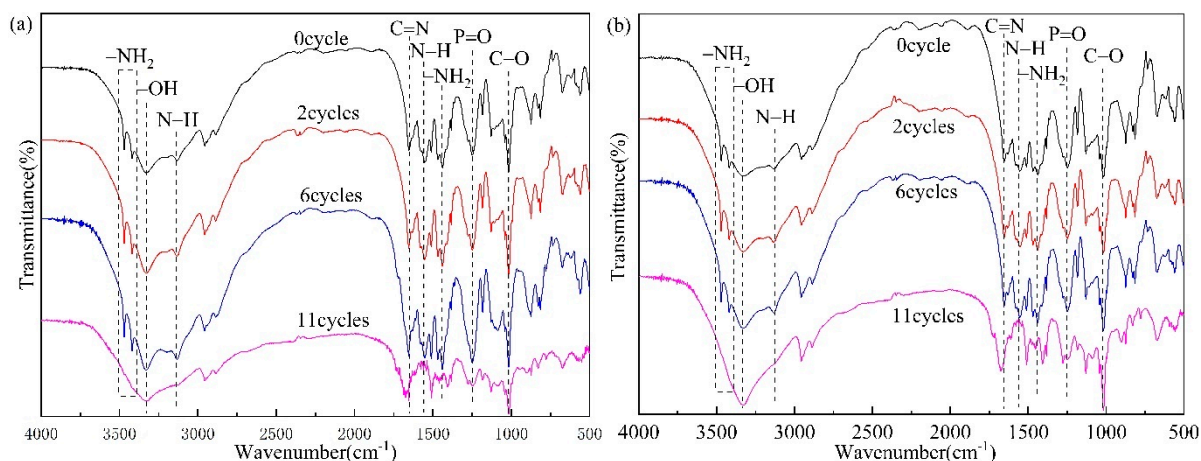


Figure 17. FTIR spectra of IFRC₀ (a) and IFRC₃ (b) after different ageing cycles.

Table 5. FTIR assignments for functional groups of IFRC₀ and IFRC₃ after different ageing cycles.

FTIR Band (cm ⁻¹)	Functional Groups	Observations	
		Intensity	Changes
1439, 3419, 3470	-NH ₂ stretching	Strong	Disappeared
1645	C=N stretching	Weak	Slightly decreased
1552, 3134	N-H stretching	Strong	Disappeared
1249	P=O stretching	Weak	Slightly decreased
1016	C-O stretching	Strong	Significantly decreased

3.7. Flame Retardant and Smoke-Suppression Mechanisms

To further study the effect of PPY-TTF on the flame retardancy and smoke suppression properties of intumescent fire-retardant coatings, the combustion processes of the cured epoxy resin, IFRC₀ and IFRC₃ samples are analyzed using a cone calorimeter, and the results are presented in Figure 18. As shown in Figure 18, a molten layer is formed at about

60 s on the surface of the coating at a radiation flux of 50 kW/m^2 . As the temperature increases, the components of the coatings interact to form an intumescent char layer, which suppresses the further decomposition of the coatings. With the increase in burning time, the formed char layers start to decompose and weaken the barrier effect on the inner coating. The cured epoxy resin starts to burn at 125 s, while the addition of IFR delays the ignition time of the coating to 372 s. More importantly, the IFRC₃ char maintains its structural integrity at 900 s, which means that the incorporation of PPY-TTF can effectively strengthen the fire resistance of the coatings and provide better protection for the substrate.

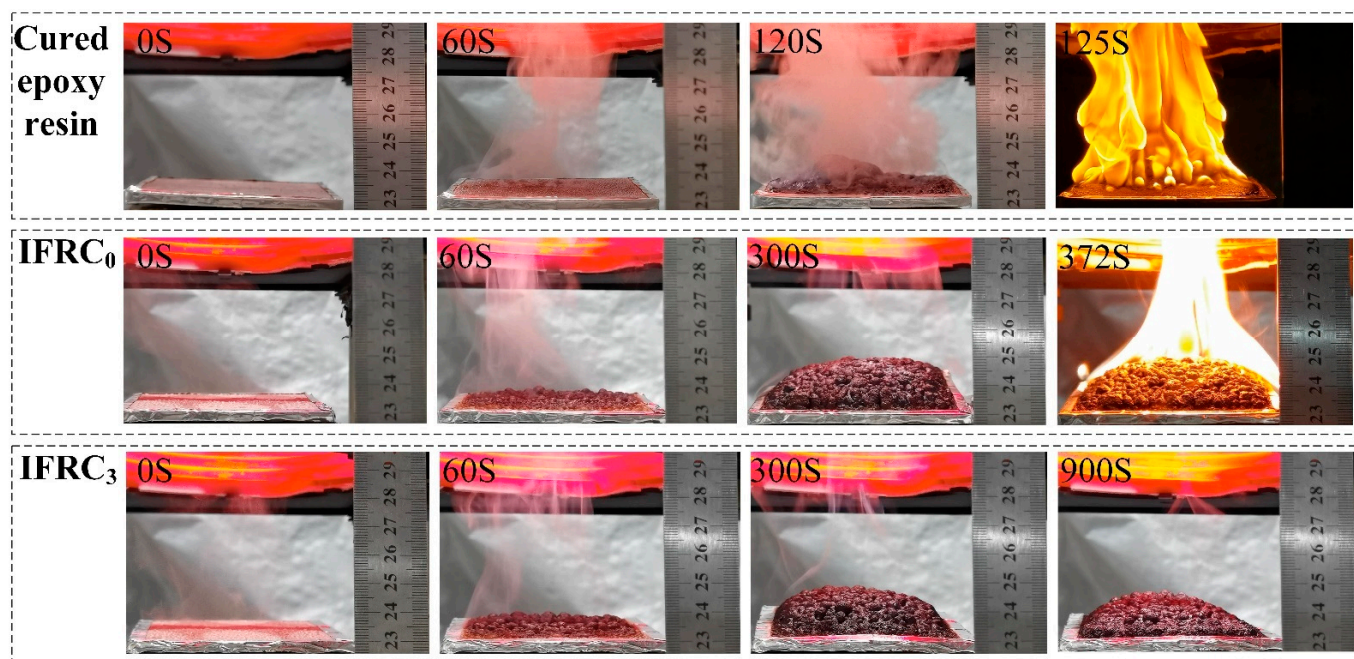


Figure 18. Digital photographs of the cured epoxy resin, IFRC₀ and IFRC₃ at expansion test.

The FTIR spectra and digital photos of IFRC₀ and IFRC₃ after different treating temperatures are depicted in Figure 19 and Table 6. When the temperature reaches $300 \text{ }^\circ\text{C}$, the $-\text{NH}_2$ ($3469, 3419 \text{ cm}^{-1}$), N-H (1552 cm^{-1}), PO_3^{2-} (1129 cm^{-1}), C-O (1015 cm^{-1}) and P-O-P ($669, 873 \text{ cm}^{-1}$) groups disappear and the P-O-C group appears at 1043 cm^{-1} [23,26–34], indicating the decomposition of APP, PER, MEL and epoxy resin at a low temperature. Besides, the decomposition temperature of the N-H group in the IFRC₃ coating is $100 \text{ }^\circ\text{C}$ lower than that of the IFRC₀ sample due to the earlier char formation of the coating. As the temperature continues to increase, the pictures reveal that the components of the intumescent fire-retardant coatings interact to form an intumescent char layer, and the main functional group peaks of the coatings in the corresponding FTIR spectra basically disappear. When the temperature reaches $800 \text{ }^\circ\text{C}$, the char residue of the IFRC₃ sample appears stronger stretching vibration peaks of P=O (1324 cm^{-1}), C-O-C (1139 cm^{-1}), P-O-C (921 cm^{-1}) and aromatic C-H (739 cm^{-1}) groups than those of IFRC₀, indicating that the presence of PPY-TTF causes the char residue to form more phosphorus-rich cross-linking structures and aromatic structures, thus improving the heat insulation and thermal stability of the char layer [35–38]. This result is consistent with the higher residual weight of IFRC₃ sample in TG analysis.

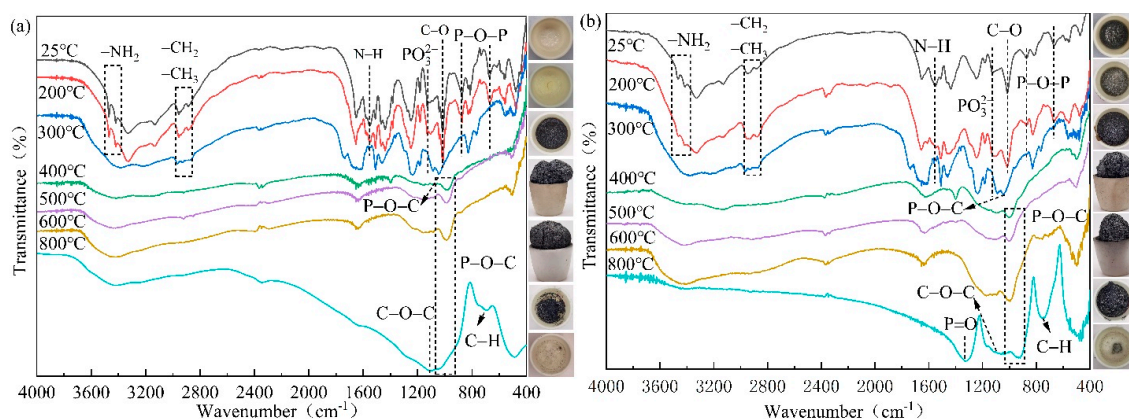


Figure 19. FTIR spectrum and digital pictures of IFRC₀ (a) and IFRC₃ (b) after different treating temperatures.

Table 6. FTIR assignments for the functional groups of the IFRC₀ and IFRC₃ after different treatment temperatures.

FTIR Band (cm ⁻¹)	Functional Groups	Observations	
		Intensity	Changes
3469, 3419	-NH ₂ stretching	Strong	Disappeared
2956, 2885	-CH ₂ stretching	Strong	Disappeared
1552	N-H stretching	Strong	Disappeared
1324	P=O stretching	Strong	New, increased
1139	C-O-C stretching	Strong	New, increased
1129	PO ₃ ²⁻ stretching	Strong	Disappeared
1043, 921	P-O-C stretching	Strong	New, increased
1015	C-O stretching	Strong	Disappeared
739	C-H deformation for benzene ring	Strong	New, increased
669, 873	P-O-P stretching	Strong	Disappeared

During the combustion process, APP is heated and decomposed to release metaphosphate, phosphate, inorganic acid and non-combustible gas, among which inorganic acid can encourage the esterification of PER into char to form a molten layer. At this stage, the introduction of PPY-TTF promotes the production of more cross-linking structures in the condensed phase. At the same time, MEL will decompose and cyclize into triazine compounds, while a large amount of non-combustible gas is released to induce the expansion of the char layer, diluting the fuel gas and weakening the burning intensity. The PPY-TTF will promote the formation of a smoother and denser protective char layer that delays the transfer of heat and mass between the fire and char layer, thus effectively suppressing the further decomposition of the coating. With the rise in temperature, the PPY-TTF contributes to the cross-linking reaction of degradation products that generate more cross-linking and aromatic structures in the condensed phase, which enhance the thermal stability and char-forming properties of coatings. However, the positive effect of PPY-TTF in the coatings is depended on its content. An excessive content of PPY-TTF may inhibit the char formation and decrease the expansion rating of the char layer, thus causing a reduction in the cooperative effect on the fire resistance and smoke suppression performance of intumescent fire-retardant coatings.

4. Conclusions

In this work, a preparation method for PPY-TTF was proposed via the in situ polymerization of pyrrole on the surface of tungsten tailing fillers, and the structures and properties of synthesized particles were characterized in detail by combining SEM-EDS, XRD, FTIR, XRF and TG analyses. Then, the PPY-TTF was applied to intumescent fire-retardant coatings as an adjuvant, and the effect of PPY-TTF on the fire resistance and anti-ageing properties of intumescent fire-retardant coatings was investigated by different analytical methods. The

results reveal that the presence of PPY-TTF enhances the fire resistance, thermal stability, char formation and smoke suppression properties of intumescent fire-retardant coatings, exhibiting super cooperative flame-retardant and smoke suppression effects. The cooperative effect of PPY-TTF in intumescent coatings is ascribed to the formation of more cross-linking and aromatic structures in the condensed phase that enhance the barrier effect of char, as supported by digital photos and SEM images. However, an excessive content of PPY-TTF will weaken the char-forming ability of the coatings, thus diminishing the excellent cooperative efficiency. In particular, the IFRC₃ sample containing 3 wt% PPY-TTF presents the best fire resistance among all samples, and has a 74.3% reduction in flame-spread rating, 30.7% reduction in total heat release, 32.9% reduction in mass loss and 32.4% reduction in smoke density rating value compared with IFRC₀. The TG analysis suggests that PPY-TTF can strengthen the char-forming ability of intumescent fire-retardant coatings, and the residual weights of IFRC₀, IFRC₁, IFRC₃, IFRC₄ and IFRC₅ at 800 °C are 26.7%, 31.6%, 34.9%, 33.5% and 30.6%, respectively. The accelerated ageing test demonstrates that an appropriate amount of PPY-TTF can improve the shielding effect and structural stability of the coatings that effectively slow down the blistering and powdering phenomenon of the coatings, thus achieving a long-term durability of the fire resistance and smoke suppression properties of the coatings. In summary, PPY-TTF provides a new strategy to utilize tungsten tailing in the fields of flame-retardant materials.

Author Contributions: F.W., conception, formal analysis, writing—review and editing; H.L., methodology, investigation, resources, validation, data curation, writing—original draft preparation; L.Y., validation, methodology, writing—review and editing, project administration, supervision; All authors have read and agreed to the published version of the manuscript.

Funding: This study received funding from the National Natural Science Foundation of China (Nos. 51906261, 51974362), the Key Research and Development Program of Hunan Province (No. 2021SK2054) and the Graduate Research and Innovation Project of Central South University (2020zzts636).

Institutional Review Board Statement: Not applicable.

Informed Consent Statement: Not applicable.

Data Availability Statement: The data presented in this study are available upon request from the corresponding author.

Conflicts of Interest: The authors declare no conflict of interest.

References

1. Schaumann, P.; Tabeling, F.; Weisheim, W. Application of intumescent coatings in steel construction. *Bautechnik* **2017**, *94*, 368–374. [[CrossRef](#)]
2. Puri, R.; Khanna, A. Intumescent coatings: A review on recent progress. *J. Coat. Technol. Res.* **2017**, *14*, 1–20. [[CrossRef](#)]
3. Xu, Z.; Xie, X.; Yan, L.; Zhou, H. Influence of carbon nanoparticle geometry on the fire resistance and anti-ageing properties of intumescent fire-retardant coatings. *Fire Mater.* **2021**, *in press*. [[CrossRef](#)]
4. Yan, L.; Xu, Z.; Wang, X. Synergistic effects of organically modified montmorillonite on the flame-retardant and smoke suppression properties of transparent intumescent fire-retardant coatings. *Prog. Org. Coat.* **2018**, *122*, 107–118. [[CrossRef](#)]
5. Xu, Z.; Chu, Z.; Yan, L.; Chen, H.; Jia, H.; Tang, W. Effect of chicken eggshell on the flame-retardant and smoke suppression properties of an epoxy-based traditional APP-PER-MEL system. *Polym. Compos.* **2019**, *40*, 2712–2723. [[CrossRef](#)]
6. Wang, F.; Liu, H.; Yan, L.; Feng, Y. Comparative Study of Fire Resistance and Anti-Ageing Properties of Intumescent Fire-Retardant Coatings Reinforced with Conch Shell Bio-Filler. *Polymers* **2021**, *13*, 2620. [[CrossRef](#)]
7. Xu, Z.; Xie, X.; Yan, L.; Feng, Y. Fabrication of organophosphate-grafted kaolinite and its effect on the fire-resistant and anti-ageing properties of amino transparent fire-retardant coatings. *Polym. Degrad. Stab.* **2021**, *188*, 109589. [[CrossRef](#)]
8. Nguyen, T.; Dao, P.; Duong, K.; Duong, Q.; Vu, Q.; Nguyen, A.; Mac, V.; Le, T. Effect of R-TiO₂ and ZnO nanoparticles on the UV-shielding efficiency of water-borne acrylic coating. *Prog. Org. Coat.* **2017**, *110*, 114–121. [[CrossRef](#)]
9. Li, Y.; Feng, Y.; Xu, Z.; Yan, L.; Xie, X.; Wang, Z. Synergistic effect of clam shell bio-filler on the fire-resistance and char formation of intumescent fire-retardant coatings. *J. Mater. Res. Technol.* **2020**, *9*, 14718–14728. [[CrossRef](#)]
10. Xu, Z.; Zhou, H.; Yan, L.; Jia, H. Comparative study of the fire protection performance and thermal stability of intumescent fire-retardant coatings filled with three types of clay nano-fillers. *Fire Mater.* **2019**, *44*, 112–120. [[CrossRef](#)]

11. Yan, L.; Xu, Z.; Liu, D. Synthesis and application of novel magnesium phosphate ester flame retardants for transparent intumescent fire-retardant coatings applied on wood substrates. *Prog. Org. Coat.* **2019**, *129*, 327–337. [[CrossRef](#)]
12. Habashy, M.; Abd-Elhady, A.; Elsad, R.; Izzularab, M. Performance of PVC/SiO₂ nanocomposites under thermal ageing. *Appl. Nanosci.* **2021**, *11*, 2143–2151. [[CrossRef](#)]
13. Dai, T.; Yang, X.; Yun, L. Conductive composites of polypyrrole and sulfonic-functionalized silica spheres. *Mater. Lett.* **2007**, *61*, 3142–3145. [[CrossRef](#)]
14. Mrah, L.; Meghabar, R. Influence of clay modification process in polypyrrole-layered silicate nanocomposite. *SN Appl. Sci.* **2020**, *2*, 155–159. [[CrossRef](#)]
15. Gan, J.; Lim, Y.; Huang, N.; Hong, N. Effect of pH on morphology and supercapacitive properties of manganese oxide/polypyrrole nanocomposite. *Appl. Surf. Sci.* **2015**, *357*, 479–486. [[CrossRef](#)]
16. Gai, L.; Han, X.; Hou, Y.; Chen, J.; Jiang, H. Surfactant-free synthesis of Fe₃O₄@PANI and Fe₃O₄@PPy microspheres as adsorbents for isolation of PCR-ready DNA. *Dalton Trans.* **2013**, *42*, 1820–1826. [[CrossRef](#)]
17. Yang, R.; Reddy, P.; Chang, C.; Chen, P. Synthesis and characterization of Fe₃O₄/polypyrrole/carbon nanotube composites with tunable microwave absorption properties: Role of carbon nanotube and polypyrrole content. *Chem. Eng. J.* **2016**, *285*, 497–507. [[CrossRef](#)]
18. Wang, H.; Yuan, X.; Wu, Y.; Chen, X.; Leng, L.; Wang, H.; Li, H.; Zeng, G. Facile synthesis of polypyrrole decorated reduced graphene oxide-Fe₃O₄ magnetic-composites and its application for the Cr(VI) removal. *Chem. Eng. J.* **2015**, *262*, 597–606. [[CrossRef](#)]
19. Maeda, S.; Gill, M.; Armes, S.; Fletcher, I. Surface Characterization of Conducting Polymer-Silica Nanocomposites by X-ray Photoelectron Spectroscopy. *Langmuir.* **1995**, *11*, 1899–1904. [[CrossRef](#)]
20. Yan, L.; Xu, Z.; Wang, X. Influence of nano-silica on the flame retardancy and smoke suppression properties of transparent intumescent fire-retardant coatings. *Prog. Org. Coat.* **2017**, *112*, 319–329. [[CrossRef](#)]
21. Khadija, E.; Shimaa, A.; Aishah, A. Synthesis and Characterization of Nano-Conducting Copolymer Composites: Efficient Sorbents for Organic Pollutants. *Molecules.* **2017**, *22*, 772. [[CrossRef](#)]
22. Shi, Y.; Wang, G. The novel silicon-containing epoxy/PEPA phosphate flame retardant for transparent intumescent fire resistant coating. *Appl. Surf. Sci.* **2016**, *385*, 456–463. [[CrossRef](#)]
23. Yang, F.; Yang, W.; Zhu, L.; Chen, Y.; Ye, Z. Preparation and investigation of waterborne fluorinated polyacrylate/silica nanocomposite coatings. *Prog. Org. Coat.* **2016**, *95*, 1–7. [[CrossRef](#)]
24. Gómez-Fernández, S.; Ugarte, L.; Peña-Rodríguez, C.; Corcuera, M.; Eceiza, A. The effect of phosphorus containing polyol and layered double hydroxides on the properties of a castor oil based flexible polyurethane foam. *Polym. Degrad. Stab.* **2016**, *132*, 41–51. [[CrossRef](#)]
25. Chang, C.; Wu, Y.; Cheng, L. Preparation of HMDS-modified silica/polyacrylate hydrophobic hard coatings on PMMA substrates. *J. Coat. Technol. Res.* **2016**, *13*, 999–1007. [[CrossRef](#)]
26. Wang, J.; Wang, G. Influences of montmorillonite on fire protection, water and corrosion resistance of waterborne intumescent fire retardant coating for steel structure. *Surf. Coat. Technol.* **2014**, *239*, 177–184. [[CrossRef](#)]
27. Wang, J.; Zhao, M. Study on the effects of aging by accelerated weathering on the intumescent fire retardant coating for steel elements. *Eng. Fail. Anal.* **2020**, *118*, 104920. [[CrossRef](#)]
28. Shi, Y.; Wang, G. The novel epoxy/PEPA phosphate flame retardants: Synthesis, characterization and application in transparent intumescent fire resistant coatings. *Prog. Org. Coat.* **2016**, *97*, 1–9. [[CrossRef](#)]
29. Zhu, F.; Xin, Q.; Feng, Q.; Liu, R.; Li, K. Influence of nano-silica on flame resistance behavior of intumescent flame retardant cellulosic textiles: Remarkable synergistic effect? *Surf. Coat. Technol.* **2016**, *294*, 90–94. [[CrossRef](#)]
30. Das, S.; Pandey, P.; Mohanty, S.; Nayak, S. Effect of nanosilica on the physicochemical, morphological and curing characteristics of transesterified castor oil based polyurethane coatings—ScienceDirect. *Prog. Org. Coat.* **2016**, *97*, 233–243. [[CrossRef](#)]
31. Makhoul, G.; Hassan, M.; Nour, M.; Abdel-Monem, Y.; Abdelkhalik, A. Evaluation of fire performance of linear low-density polyethylene containing novel intumescent flame retardant. *J. Therm. Anal. Calorim.* **2017**, *130*, 1031–1041. [[CrossRef](#)]
32. Ullah, S.; Ahmad, F. Effects of zirconium silicate reinforcement on expandable graphite based intumescent fire retardant coating. *Polym. Degrad. Stab.* **2014**, *103*, 49–62. [[CrossRef](#)]
33. Deng, C.; Du, S.; Zhao, J.; Shen, Z.; Deng, C.; Wang, Y. An intumescent flame retardant polypropylene system with simultaneously improved flame retardancy and water resistance. *Polym. Degrad. Stab.* **2014**, *108*, 97–107. [[CrossRef](#)]
34. Zheng, Z.; Liu, Y.; Zhang, L.; Wang, H. Synergistic effect of expandable graphite and intumescent flame retardants on the flame retardancy and thermal stability of polypropylene. *J. Mater. Sci.* **2016**, *51*, 5857–5871. [[CrossRef](#)]
35. Hu, Q.; Peng, P.; Peng, S.; Liu, J.; Liu, X.; Zou, L.; Chen, J. Flame-retardant epoxy resin based on aluminum monomethylphosphinate. *J. Therm. Anal. Calorim.* **2017**, *128*, 201–210. [[CrossRef](#)]
36. Nikolic, M.; Nguyen, H.; Dugaard, A.; Löf, D.; Mortensen, K.; Barsberg, S.; Sanadi, A. Influence of surface modified nano silica on alkyd binder before and after accelerated weathering. *Polym. Degrad. Stab.* **2016**, *126*, 134–143. [[CrossRef](#)]
37. Hu, X.; Wang, G.; Huang, Y. Study on the preparation and properties of novel transparent fire-resistive coatings. *J. Coat. Technol. Res.* **2013**, *10*, 717–726. [[CrossRef](#)]
38. Wang, G.; Huang, Y.; Hu, X. Synthesis of a novel phosphorus-containing polymer and its application in amino intumescent fire resistant coating. *Prog. Org. Coat.* **2013**, *76*, 188–193. [[CrossRef](#)]